Nano Energy (2014) 8, 291–296

Available online at www.sciencedirect.com

ScienceDirect

journal homepage: www.elsevier.com/locate/nanoenergy

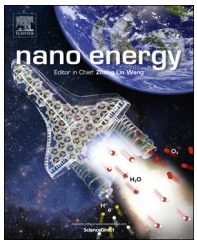

RAPID COMMUNICATION

Excellent piezoelectric and electrical properties of lithium-doped ZnO nanowires for nanogenerator applications

Yu-Tsui Chang[a,1], Jui-Yuan Chen[a,1], Tzu-Ping Yang[b], Chun-Wei Huang[a], Chung-Hua Chiu[a], Ping-Hung Yeh[c], Wen-Wei Wu[a,*]

[a]Department of Materials Science and Engineering, National Chiao Tung University, Hsinchu 30010, Taiwan
[b]Department of Materials Science and Engineering, National Tsing Hua University, Hsinchu 30013, Taiwan
[c]Department of Physics, Tamkang University, Tamsui, New Taipei City 25137, Taiwan

Received 12 March 2014; received in revised form 29 May 2014; accepted 12 June 2014
Available online 23 June 2014

KEYWORDS
ZnO;
Lithium-doped;
Piezoelectric property;
Hydrothermal method;
Magnetization

Abstract
The well-aligned Li-doped zinc oxide nanowires (ZnO NWs) were successfully grown on Si substrates with seed layer by the hydrothermal method. The presence of Li in ZnO NWs is confirmed through EELS spectrum analysis. The acceptor energy level of the Li dopant is estimated to be 93.6 meV from the temperature-dependent PL spectra. From the SQUID measurements, the coercivity and saturation magnetization of the Li-doped ZnO NWs at room temperature are found to be 166 Oe and 9.64 memu/g, respectively. Additionally, the Li-doped ZnO NWFET confirms that the NWs were p-type with a high carrier mobility of 14.59 $cm^2/V\,s$ and an effective hole carrier concentration of $1.13 \times 10^{17}\ cm^{-3}$. The piezoelectric response of the Li-doped ZnO NWs produces much higher piezoelectric output current, voltage, and power than pure ZnO NWs. These results indicated that p-type ZnO NWs are a promising candidate for nanogenerator devices.

Introduction

Zinc oxide is a wurtzite crystal with a hexagonal structure; its wide band gap of about 3.37 eV, high excitation binding energy of about 60 meV at room temperature make it a potential semiconductor material for optoelectronic devices

*Corresponding author. Tel.: +886 3 5712121 55395.
E-mail address: wwwu@mail.nctu.edu.tw (W.-W. Wu).
[1]These authors have equally contributed.

http://dx.doi.org/10.1016/j.nanoen.2014.06.014
2211-2855/

such as light-emitting diodes [1] and ultraviolet (UV) lasers [2]. In particular, compared to other materials, the morphology of one-dimensional zinc oxide nanostructure is diversification [3], which has attracted great interest as a promising material for nanodevices due to their specific physical properties. It has been reported that ZnO NW has various applications in electronics, electromechanical, and electrochemical nanodevices, including field-emission devices, solar cells, and piezoelectric nanogenerators [4]. However, because of intrinsic n-type characteristic, the electrical application of ZnO-based device was hindered, resulting in considerable effort which has been dedicated toward the development of p-type ZnO NWs [5–8].

Wide band gap materials usually show a poor doping efficiency due to the feature of deep acceptor energy level. Among various dopant candidates, several reports have indicated that Li atoms can act as shallow acceptors in substantial forms of Zn sites (LiZn) [9]. Li is considered to have a smaller strain effect and to be highly soluble in ZnO [10] because it has the smallest ionic radius (0.76 Å) which is close to that of Zn (0.74 Å) compared to other group I elements. Moreover, the substitutive Li atom will stabilize zinc vacancies that induce magnetic moment. Thus, this contributes to an exceptional class of magnetoelectric materials with immense potential for spintronic and magneto-optic devices [11].

The properties of optical and field emission in Li-doped ZnO have been studied by several researches [12,13]; however, for the first time, we report the piezoelectric study of Li-doped ZnO NWs here. We have demonstrated the enhanced output current of Li-doped ZnO, showing potential applications in the field of nanogenerator devices. The (100) silicon substrates were cleaned by a diluted HF solution cleaning process to remove native oxide. Ga-doped ZnO seed layers (100 nm thick) were prepared using the plasma sputtering system. Next, the Li-doped ZnO NWs were synthesized in an aqueous solution of 5 mM aqueous zinc acetate, hexamethylenetetramine, and 20 mM lithium acetate in a digital water bath at a constant temperature of 85 °C for 12 h in an oven. Finally, the NWs were annealed under a constant oxygen partial pressure of 0.5 Torr at 550 °C for 1 min by the RTA system.

The Li-doped ZnO NWs arrays grown by the hydrothermal method were investigated with scanning electron microscope (JEOL JSM-6500F), transmission electron microscope (JEOL JEM-2100F), and X-ray diffraction (Bruker D2 phaser) measurements for structural analysis. In addition, an electron energy loss spectroscopy (EELS) measurement using scanning transmission electron microscopy (STEM) operated at 200 kV was performed to provide evidence for the existence of lithium in ZnO NWs. A temperature-dependent PL with 325 nm He–Cd laser was used to study the optical property of ZnO NWs. The ferromagnetic property was measured by Superconducting Quantum Interference Device (MPMS-XL). The electrical properties were measured by semiconductor analyzers (Agilent B1500A) at room temperature in ambient conditions. However, the piezoelectric response of the ZnO NWs was measured by C-AFM (NT-MDT Solver P47).

To improve the aspect ratio and length of Li-doped ZnO NWs, multistep growth was adopted to synthesize NWs with a higher aspect ratio as shown in Figure 1(a). After completing growth cycles 5 times with the same growth conditions described above, the well-aligned Li-doped ZnO NWs arrays with 1 μm and 10 μm in length were controlled by one step and five steps, respectively. The length of the NWs was up to 10 μm with uniform diameters in the range of 200–300 nm after multistep growth. The lateral growth was suppressed by adding dilute nitric acid in solution [14]. The aspect ratio of the Li-doped ZnO NWs increases prominently from 9.8 to 33.3 μm with increase in the steps of growth, resulting in a higher surface-to-volume ratio. In Figure 1(b), the low

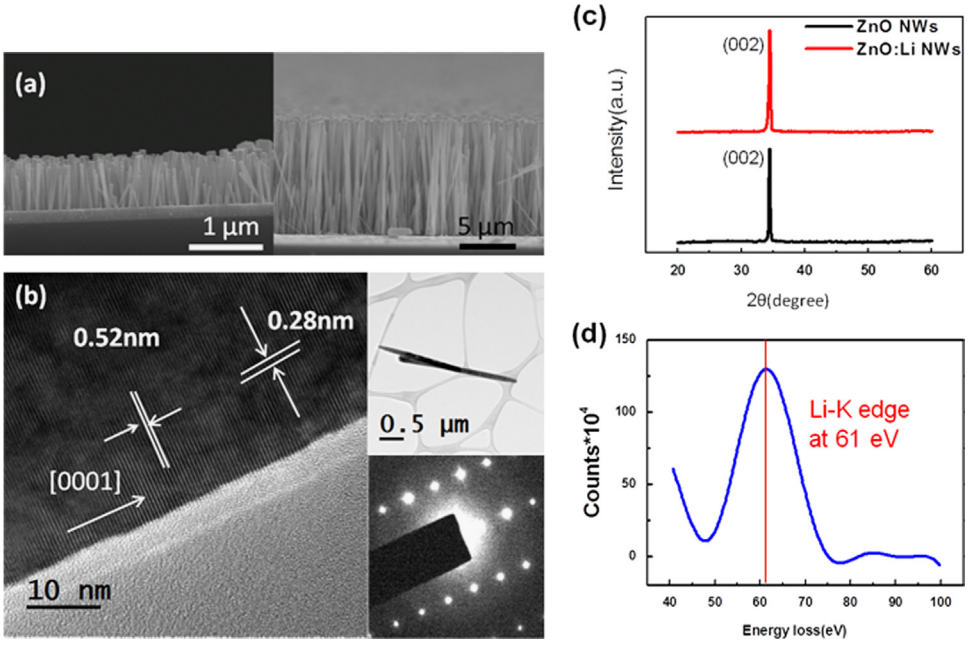

Figure 1 (a) FESEM image of Li-doped ZnO NWs grown on Si substrate (one-step and multi-step). (b) TEM image of single Li-doped ZnO NW, the corresponding HRTEM image and SAED pattern. (c) XRD spectra of Li-doped and pure ZnO NWs. (d) EELS spectrum of single Li-doped ZnO NW, the extracted signal showed a Li K edge peak at 61 eV.

magnification TEM image of a Li-doped ZnO single NW exhibits a diameter of about 120 nm and a length of about 2.4 μm. The high-resolution TEM (HRTEM) image clearly shows the atomically resolved wurzite ZnO single crystal. The growth direction was also along the ⟨0001⟩ direction, as observed from the corresponding selected area electron diffraction (SEAD) pattern. In Figure 1(c), XRD spectrum shows that the relatively strong (002) peak demonstrates the preferred orientation of the lithium-doped ZnO NWs and pure ZnO NWs, which were consistent with the result of TEM. Neither zinc nor lithium characteristic peaks were observed from the XRD spectra. Figure 1(d) shows the EELS spectrum of the single lithium-doped ZnO NW, which clearly demonstrated Li K edge peaks at 61 eV, confirming the appearance of Li in ZnO NW.

Temperature-dependent PL measurements were performed to further infer the emission evolution related to lithium dopant activation. The low-temperature PL spectra of aligned lithium-doped ZnO NWs and pure ZnO NWs at 10 K are illustrated in Figure 2(a), which reveal a clear red shift of near-band-edge emission in lithium-doped ZnO NWs and ZnO NWs. This result demonstrates that lithium atoms in ZnO system reduce the value of band gap, the same result was also found in UV-vis measurement (S1, 2 details in the Supporting information). Figure 2(b) shows the PL emission spectra of the lithium-doped ZnO NWs at temperatures ranging from 10 to 250 K. The intensity of PL spectra decreases as temperature rises, which can be attributed to thermal vibration suppressing the emission of photoluminescence. The near-band-edge red shifted with increasing temperature because neutral acceptor-bound exciton peak dominated at low temperature whereas the free exciton transition dominated at room temperature [15]. Figure 2(c) is an Arrhenius plot of the integrated PL intensity of the A°X emission as a function of temperature for the lithium-doped ZnO NWs. The temperature-dependent activated behaviors of A°X emission were described as follows:

$$I(T) = \frac{I_0}{1 + C\exp(-E_b^{A^\circ X}/k_B T)}$$

where I_0 is the emission intensity at 10 K taken to be approximately the same as the experimentally measured value at T=10 K, C is a free fitting parameter, kB is the Boltzmann constant, T is the temperature, and $E_b^{A^\circ X}$ is the binding energy between the free exciton and acceptor [16]. As shown in Figure 2(c), a fitting value of $E_b^{A^\circ X} = 9.36$ meV. According to the Haynes rule, [17] there is a linear dependence between $E_b^{A^\circ X}$ and EA (acceptor level), and the value is about 0.1 in the ZnO material system [15]. Therefore, the acceptor level of the lithium dopant was estimated about 93.6 meV as a shallow acceptor level.

The origin of ferromagnetism in dilute magnetic Li-doped ZnO semiconductor is zinc vacancy. Theoretical studies have been carried out to investigate the mechanisms of ferromagnetism associated with defects. The results of first-principle calculations indicated that neutral oxygen vacancy in ZnO is nonmagnetic [18], whereas zinc vacancy does lead to magnetism [19]. Cation vacancies introduce local magnetic moments as well as holes to the host semiconductor, and ferromagnetism in such a DMS (diluted magnetic semiconductors) can be mediated by holes. Moreover, it has been evidenced that cation vacancies stabilization and holes increase can contribute to the enhanced ferromagnetism in a ZnO system [20]. In this study, the presence of lithium would reduce the formation energy of zinc vacancy. Therefore, such lower energy stabilizes the zinc vacancy and leads to dilute magnetism (each zinc vacancy carries a

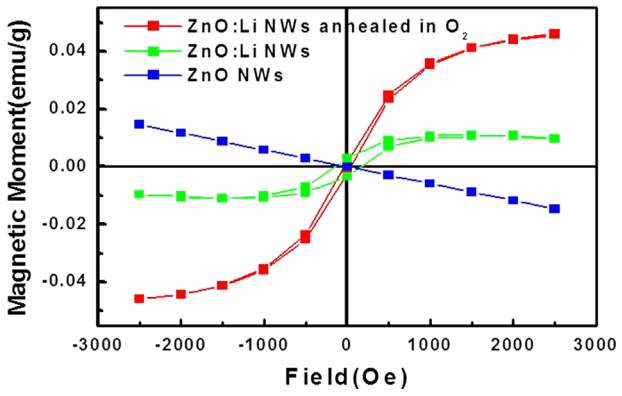

Figure 3 Hysteresis loops of Li-doped ZnO NWs measured at room temperature. The Li-doped ZnO NWs after annealing under a constant oxygen partial pressure of 0.5 Torr at 550 °C result in an increase in M_S. Pure ZnO NWs exhibit diamagnetic characteristic.

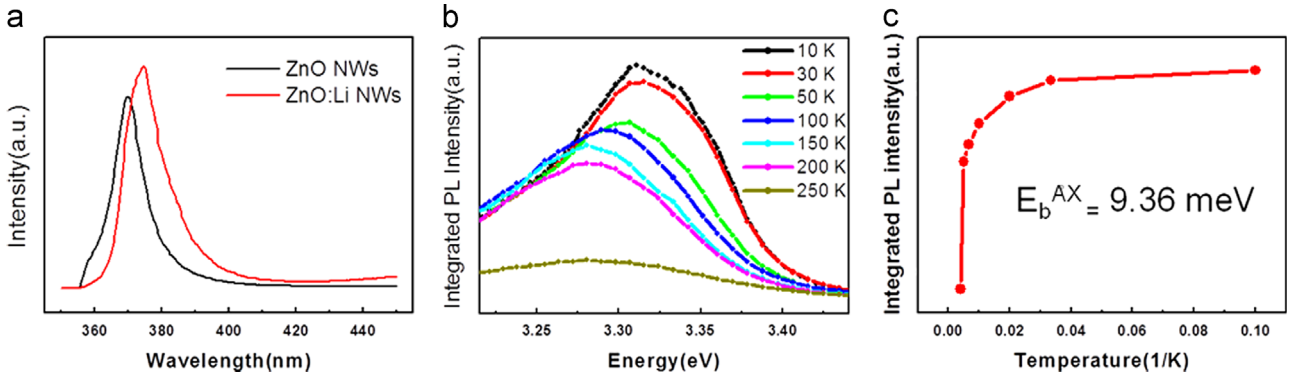

Figure 2 Optical properties of Li-doped ZnO NWs. (a) PL spectra of Li-doped ZnO NWs and ZnO NWs at 10 K. (b) Temperature-dependent PL spectra of Li-doped ZnO NWs over a temperature range of 10–250 K. (c) Integrated intensity of the A◦X emission as a function of 1/T for Li-doped ZnO NWs.

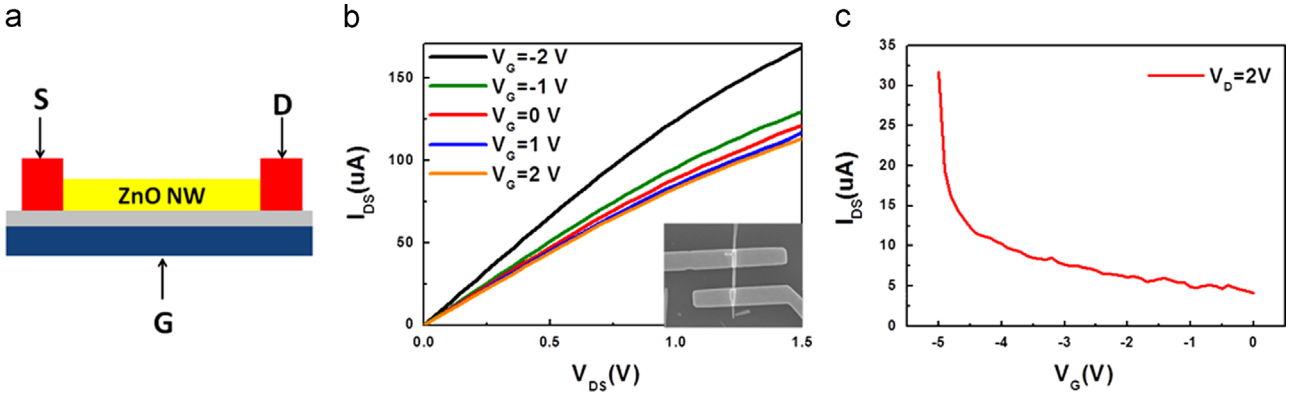

Figure 4 Electrical properties of a Li-doped ZnO NW. (a) The schematic diagram of back gate FET. (b) Output properties of a back gate field-effect transistor with a Li-doped ZnO NW. (c) Transistor properties of NWFET at V_{DS}=2 V.

magnetic moment of 1.33 μB), whereas lithium itself is nonmagnetic. By SQUID measurements, as shown in Figure 3, the coercivity and saturation magnetization of the Li-doped NWs at room temperature were 166 Oe and 9.64 memu/g, respectively. In addition, we also observed that the lithium-doped ZnO NWs after annealing at 550 °C under oxygen-rich condition result in an increase in saturation magnetization to 46.1 memu/g. It indicates that the zinc vacancies would prefer to be formed and stabilized as the oxygen chemical increases [21].

In order to characterize the electrical performance of lithium-doped ZnO NWs, single NW-based field-effect transistors (NWFET) were fabricated to study the electrical transport properties. Lithium-doped ZnO NWs were first dispersed on a heavily doped Si wafer with silicon oxide on the top, which served as the back-gate electrode as shown in Figure 4(a). Contact electrodes, nickel (30 nm) and gold (120 nm) were subsequently deposited by the processes of e-beam lithography and e-gun deposition. The resistivity of single Li-doped ZnO NW was investigated (S3, details in the Supporting information). Figure 4(b), c shows typical source-to-drain current (I_{DS})-voltage (V_{DS}) p-type outputs at different gate voltages (V_G) from −2 to 2 voltage and transfer characteristics from the device, where the measurement was performed at room temperature in ambient conditions. It is clear that all $I_{DS}-V_{DS}$ curves were almost linear, indicating that ohmic contacts were formed between the lithium-doped ZnO NW and Ni/Au electrodes. The field-effect mobility of lithium-doped ZnO NW can be estimated using the following formula [22-23]:

$$\mu = \frac{dI_{DS}L^2}{dV_G C}$$

where dI_{DS}/d_{VG} is the transconductance and C is the capacitance. The capacitance is given by

$$C = \frac{2\pi\varepsilon_{SiO_2}\varepsilon_0 L}{\ln(4h/d)}$$

where h is the thickness of the gate oxide layer (200 nm), L is the channel length (1 μm), and d is the NW diameter (174 nm). ε_{SiO_2} is the dielectric constant of the SiO_2 gate oxide (3.9), ε_0 is the dielectric permittivity. The NWFET has a high carrier mobility of 14.59 $cm^2 V^{-1} s^{-1}$ and the effective hole carrier concentration is calculated to be about 1.13×10^{17} cm^{-3} from the following equation: [23]

$$p = \frac{V_{th}C}{q\pi L(d/2)^2}$$

where q is the hole charge and V_{th} is the threshold voltage. The NWFET results demonstrate that the channel of Li-doped ZnO NW shows p-type conductivity characteristic.

Because of non-central symmetric feature in the ZnO wurtzite structure, the cations and anions are tetrahedrally coordinated and the centers of the positive ions and negative ions overlap with each other under strain-free conditions. When external stress was applied, the center of the cations and anions was relatively displaced, and produced a dipole moment. The constructive sum of the dipole moments results in a macroscopic potential, which is the origin of piezoelectricity [24,25]. Here, the piezoelectric response of the lithium-doped ZnO NW was measured using AFM with a Pt-coated silicon tip and the illustration is shown in Figure 5(a). The Indium island served as the bottom electrode with low resistance. In the AFM contact mode, a constant normal force was kept between the tip and the sample surface. The output current across an AFM load of resistance R=20 MΩ was continuously monitored as the tip scanned across the ZnO NWs array, with the Ga-doped ZnO seed layer acting as the conductive film on the substrate and no external current was applied in the experiment. Both the topography (blue line) and the corresponding output current (black line) images across the load were recorded simultaneously in Figure 5(b,c). It can be observed that the lithium-doped ZnO NWs produce much higher output current (8 nA) than pure ZnO NWs (1.6 nA). The corresponding output voltage and power of single Li-doped ZnO NWs were about 160 mV and 260 pW, respectively. The piezoelectric property with different doping elements in nanowires is included in the Supporting information Table S1 [4,6,24,27]. We suppose also that lithium atoms in substantial forms of zinc sites will change the structure of the ZnO system to produce coupling in piezoelectric/magnetostrictive effect to increase the dipole moment [25-27].

Conclusion

In summary, well-aligned Li-doped ZnO NWs with [0001] growth direction have been successfully synthesized by the

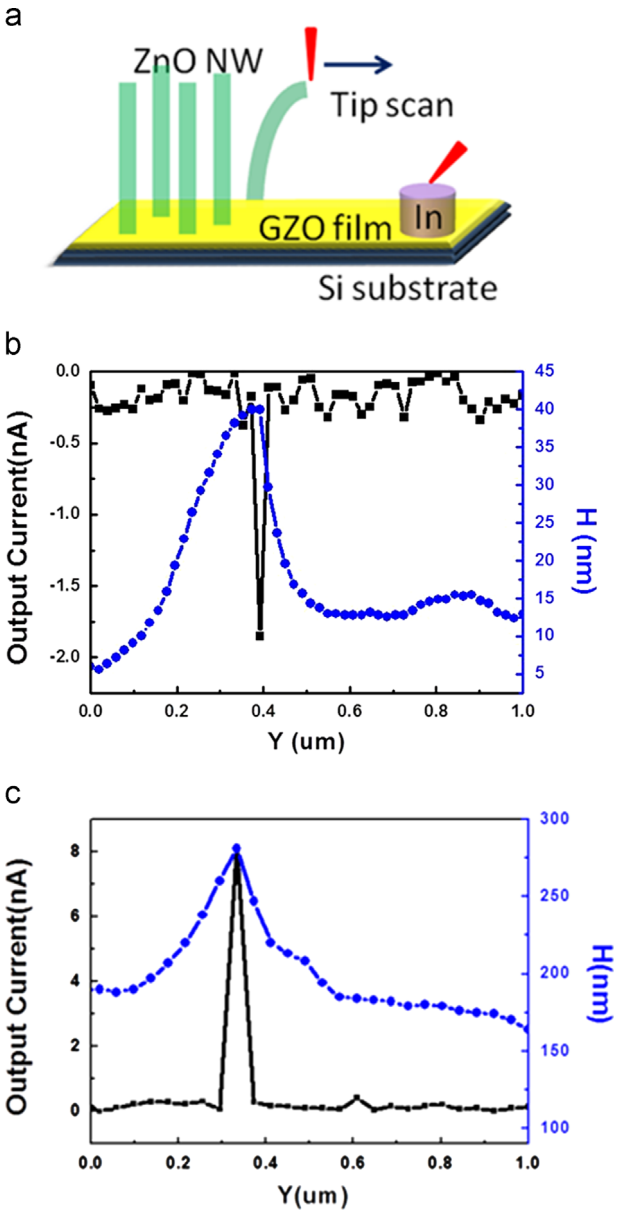

Figure 5 (a) Experimental setup for piezoelectricity measurement by deforming a NW with a conductive AFM tip. (b) Line profiles from the topography (blue) and output current (black) images across a ZnO NW. (c) Line profiles from the topography (blue) and output current (black) images across a Li-doped ZnO NW.

multiple-step hydrothermal method. The acceptor energy level of the Li dopant was 93.6 meV as measured by the temperature-dependent PL spectra. From SQUID measurements, the Hc and M_S of the Li-doped NWs at room temperature were 166 Oe and 9.64 memu/g, respectively. The electron transport property of Li-doped ZnO NWFET confirms that the single NW is p-type with a high carrier mobility of 14.59 $cm^2/V\,s$ and an effective hole carrier concentration of $1.13 \times 10^{17}\,cm^{-3}$. The piezoelectric response of the single Li-doped ZnO NW produces much higher piezoelectric output current than pure ZnO NW. Also, the interesting result of ferromagnetic property makes Li-doped ZnO NWs a promising material in the field of DMSs. Furthermore, with superior properties and incredibly high output current, voltage and power, Li-doped ZnO NWs have significant potential in applications of highly efficient nanogenerators.

Acknowledgments

The authors would like to acknowledge the support by the National Science Council Taiwan (Grant no. NSC 100-2628-E-009-023-MY3 and MOST 103-3113-E-009-004).

Appendix A. Supporting information

Supplementary data associated with this article can be found in the online version at http://dx.doi.org/10.1016/j.nanoen.2014.06.014.

References

[1] W.I. Park, G.C. Yi, Adv. Mater. 16 (2004) 87–90.
[2] M.H. Huang, S. Mao, H. Feick, H. Yan, Y. Wu, H. Kind, E. Weber, R. Russo, P. Yang, Science 292 (2001) 1897–1899.
[3] Z.L. Wang, Mater. Today 7 (2004) 26–33.
[4] Z.L. Wang, J. Song, Science 312 (2006) 242–246.
[5] X. Yang, A. Wolcott, G. Wang, A. Sobo, R.C. Fitzmorris, F. Qian, J.Z. Zhang, Y. Li, Nano Lett. 9 (2009) 2331–2336.
[6] M.-P. Lu, J. Song, M.-Y. Lu, M.-T. Chen, Y. Gao, L.-J. Chen, Z.L. Wang, Nano Lett. 9 (2009) 1223–1227.
[7] X. Fang, J. Li, D. Zhao, D. Shen, B. Li, X. Wang, J. Phys. Chem. C 113 (2009) 21208–21212.
[8] P. Ruankham, T. Sagawa, H. Sakaguchi, S. Yoshikawa, J. Mater. Chem. 21 (2011) 9710–9715.
[9] C.H. Park, S.B. Zhang, S.-H. Wei, Phys. Rev. B 66 (2002) 073202.
[10] E.-C. Lee, K.J. Chang, Phys. Rev. B 70 (2004) 115210.
[11] S. Chawla, K. Jayanthi, R.K. Kotnala, Phys. Rev. B 79 (2009) 125204.
[12] D. Uki, H. Ohnishi, T. Yamaguchi, Y. Takemori, A. Koizumi, S. Fuchi, T. Ujihara, Y. Takeda, J. Cryst. Growth 298 (2007) 69–72.
[13] N.R. Aghamalyan, R.K. Hovsepyan, N.R. Aghamalyan, S.I. Petrosyan, J. Contemp. Phys. 44 (2009) 29–35.
[14] X. Yan, Z. Li, R. Chen, W. Gao, Cryst. Growth Des. 8 (2008) 2406–2410.
[15] F.X. Xiu, Z. Yang, L.J. Mandalapu, D.T. Zhao, J.L. Liu, W.P. Beyermann, Appl. Phys. Lett. 87 (2005) 152101.
[16] S.H. Lee, J.S. Lee, W.B. Ko, J.I. Sohn, S.N. Cha, J.M. Kim, Y.J. Park, J.P. Hong, Appl. Phys. Express 5 (2012) 095002–095004.
[17] M. Leroux, N. Grandjean, B. Beaumont, G. Nataf, F. Semond, J. Massies, P. Gibart, J. Appl. Phys. 86 (1999) 3721–3728.
[18] C.H. Patterson, Phys. Rev. B 74 (2006) 144432.
[19] Q. Wang, Q. Sun, G. Chen, Y. Kawazoe, P. Jena, Phys. Rev. B 77 (2008) 205411.
[20] H.-X. Gao, J.-B. Xia, J. Appl. Phys. 111 (2012) 093902.
[21] J.B. Yi, C.C. Lim, G.Z. Xing, H.M. Fan, L.H. Van, S.L. Huang, K.S. Yang, X.L. Huang, X.B. Qin, B.Y. Wang, T. Wu, L. Wang, H.T. Zhang, X.Y. Gao, T. Liu, A.T.S. Wee, Y.P. Feng, J. Ding, Phys. Rev. Lett. 104 (2010) 137201.
[22] J. Goldberger, D.J. Sirbuly, M. Law, P. Yang, J. Phys. Chem. B 109 (2004) 9–14.

[23] J. Lee, S. Cha, J. Kim, H. Nam, S. Lee, W. Ko, K.L. Wang, J. Park, J. Hong, Adv. Mater. 23 (2011) 4183–4187.
[24] Z.L. Wang, Nano Today 5 (2010) 540–552.
[25] K.C. Pradel, W. Wu, Y. Zhou, X. Wen, Y. Ding, Z.L. Wang, Nano Lett. 13 (2013) 2647–2653.
[26] N. Lei, T. Devolder, G. Agnus, P. Aubert, L. Daniel, J.-V. Kim, W. Zhao, T. Trypiniotis, R.P. Cowburn, C. Chappert, D. Ravelosona, P. Lecoeur, Nat. Commun. 4 (2013) 1378.
[27] S.S. Lin, J.H. Song, Y.F. Lu, Z.L. Wang, Nanotechnology 20 (2009) 365703–365708.

Yu-Tsui Chang received her M.S. degree in Materials Science and Engineering from National Chiao Tung University, Taiwan in 2013. Her main research interest include synthesis of ZnO nanowires, fabrication of nanodevices, and theoretical calculation of piezotronic.

Jui-Yuan Chen is a Ph.D. candidate in Materials Science and Engineering at National Chiao Tung University. His main research interests are preparation and applications of metal-oxide nanodevices, in situ TEM investigation the nanostructures for micro/nano-memory systems.

Tzu-Ping Yang received his M.S. degree in Materials Science and Engineering from National Tsing Hua University, Taiwan in 2013. His main research interests are synthesis of metal-oxide thin film and fabrication of nanodevices.

Chun-Wei Huang received his M.S. degree in Materials Science and Engineering from National Taiwan Ocean University, Taiwan in 2009. He is a Ph.D. candidate in Materials Science and Engineering at National Chiao Tung University. His main research interests are preparation and applications of ZnO nanodevices, in situ TEM investigation for nanodevices.

Chung-Hua Chiu is a Ph.D. candidate in Materials Science and Engineering at National Chiao Tung University. His main research interests are preparation and applications of metal-oxide nanodevices and analysis of the nanostructures for micro/nano-memory systems.

Ping-Hung Yeh received his Ph.D. degree in Materials Science and Engineering from National Tsing Hua University, 2006. Then he worked as Postdoctoral Fellow (2006–2007) at Materials Science and Engineering, National Tsing Hua University. After his Postdoctoral Fellowship, he worked in Georgia Institute of Technology as a research scientist from 2007–2009. He joined in Department of Physics, Tamkang University from 2009. His main research interests are synthesis of ZnO nanowires, fabrication of nanodevices, and nanosensor.

Wen-Wei Wu received his Ph.D. degree in Materials Science and Engineering from National Tsing Hua University, 2003. Then he worked as Postdoctoral Fellow (2003–2008) at Materials Science and Engineering, National Tsing Hua University. He joined in Materials Science and Engineering, National Chiao Tung University from 2008. His main research interests are in situ TEM investigation of dynamical changes in nanostructured materials, synthesis metal silicide thin films and nanostructures, and metallization on Si and Si–Ge alloy.